(M = Mo), 12125-77-8; V (M = W), 12128-81-3; VI (M = Cr), 90624-11-6; VI (M = Mo), 90624-12-7; VI (M = W), 90624-13-8; VII, 90624-14-9; VIII (M = Mo), 17731-95-2; VIII (M = W), 30958-95-3; IX (M = Mo), 90624-15-0; IX (M = W), 90624-16-1; X, 90624-17-2; XI (M = Mn), 90624-18-3; XII (M = Mn), 90624-19-4; XII (M = Re), 90624-20-7; XIII, 90624-21-8; XIV, 90624-22-9; XV, 90624-23-0; XVI, 90624-24-1; XVII, 90624-25-2; XVIII, 90624-26-3; $Cr(CO)_6$, 13007-92-6; $Mo(CO)_6$, 13939-06-5; $W(CO)_6$, 14040-11-0; $Mn_2(CO)_{10}$, 10170-69-1; $Re_2(CO)_{10}$, 14285-68-8; $C_5H_5Mn(CO)_3$, 12079-65-1; $Fe_2(CO)_9$, 15321-51-4; $Fe(CO)_5$, 13463-40-6; $[C_5H_5Fe(CO)_2]_2$, 12154-95-9; $Ni(CO)_4$, 13463-39-3; $[C_5H_5NiCO]_2$, 12170-92-2.

Contribution from the Departments of Chemistry, Northwestern University, Evanston, Illinois 60201, and Oklahoma State University, Stillwater, Oklahoma 74078

Synthesis, Structure, and Chemistry of Sterically Crowded Metal Carbonyl Cluster Compounds: $[Fe_3M(CO)_{14}]^{2-}$ (M = Cr, Mo, W)

COLIN P. HORWITZ,[1a] ELIZABETH M. HOLT,*[1b] and DUWARD F. SHRIVER*[1a]

Received October 21, 1983

Despite previous indications in the literature that tetrahedral $M_4(CO)_{14}$ might be too crowded to be stable, the series $[Fe_3M(CO)_{14}]^{2-}$ (M = Cr, Mo, W) was synthesized by the interaction of $[Fe_3(CO)_{11}]^{2-}$ with $M(CO)_3(CH_3CN)_3$. The objective in synthesizing these sterically crowded compounds was to induce metal–metal bond breaking and a concomitant η^2-CO interaction. The structure of the compound in which M = Cr was determined by single-crystal X-ray diffraction. In contrast with the desired M–M scission, the metal framework is pseudotetrahedral with Fe–Cr distances averaging 2.633 (25) Å and Fe–Fe distances averaging 2.656 (3) Å. The latter distances are about 0.1 Å longer than expected from Fe–Fe distances in other clusters. The polygon formed by the carbonyl carbon atoms may be described as a hexacapped rectangular antiprism. Model calculations of strain energies in this compound indicate that the C–C repulsive potential, which successfully describes nonbonding forces for graphite and organic compounds, overestimates the nonbonded C–C repulsions in metal carbonyls. Strain energy calculations lead us to propose a modified potential function for C···C interactions in metal carbonyls. The reactions of the $[Fe_3M(CO)_{14}]^{2-}$ series with electrophiles, H^+ and CH_3^+, were explored, with the thought that these might induce M–M bond breaking, but this appears not to be the case. Crystallographic data for $[PPN]_2[Fe_3Cr(CO)_{14}]$: $P\bar{1}$ triclinic space group, a = 13.428 (5) Å, b = 17.734 (5) Å, c = 18.254 (9) Å, α = 95.46 (3)°, β = 105.74 (3)°, γ = 69.82 (2)°, Z = 2.

Introduction

Steric effects are frequently invoked in inorganic chemistry; however, there is comparatively little quantitative understanding of the subject. The greatest progress has been made in the area of ring conformation for metal chelate complexes, where it has been possible to build on the methods of molecular mechanics developed for organic molecules.[2] For metal phosphine and related complexes, steric interactions may be approximated by effective cone angles for the ligands,[3] which can be used to systematize phosphine substitution reactions, oxidative-addition reactions, and the like. Recent investigations have shown that the disposition of CO ligands in metal cluster carbonyl compounds can be described with reasonable accuracy by a model based on ligand–ligand repulsions.[4] At the present stage of development, this model requires a relatively symmetrical metal framework in which M–M and M–C energies are reasonably constant.

The effects of CO ligand–ligand repulsions were discussed by Doedens and Dahl,[5] who suggested that the CO ligands in $[Fe_4(CO)_{13}]^{2-}$ (I) are in such close proximity that there is no room to accommodate the 14th CO required for the formation of the isoelectronic neutral carbonyl, $Fe_4(CO)_{14}$.[5] Mingos has reached a similar conclusion for this sytem, based on the effective cone angle of CO, and his treatment predicts that $M_4(CO)_{14}$ clusters with tetrahedral metal frameworks should be strained for the second and third transition series as well.[6] Even the introduction of a "hydride" ligand to produce $[H\text{-}Fe_4(CO)_{13}]^-$ (II) results in a drastic rearrangement, which has been attributed to steric effects.[7] As illustrated in eq 1, the protonation of $[Fe_4(CO)_{13}]^{2-}$ (I) leads to the scission of an Fe–Fe bond with the formation of the butterfly compound II.

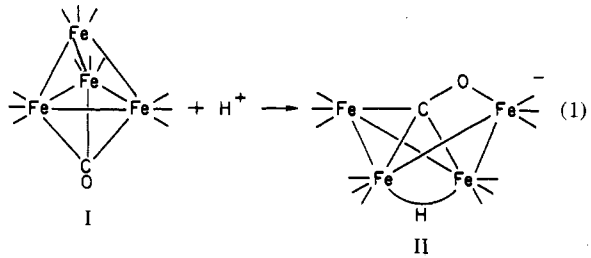

I II

Compound II is of great interest because it contains an η^2-CO ligand, which bridges the wing tips and contributes the two additional cluster valence electrons needed when the Fe–Fe bond is broken. The η^2-CO bonding mode is very interesting because it may occur as a precursor to the scission of CO on the surface of catalysts for Fischer–Tropsch and methanation.[8] Furthermore, an η^2-CO is strongly implicated in the proton-induced reduction of CO in metal cluster chemistry.[9,10] In the present research we sought to prepare $[M_4(CO)_{14}]^{2-}$

(1) (a) Northwestern University. (b) Oklahoma State University.
(2) Hawkins, C. J. "Absolute Configuration of Metal Complexes"; Wiley-Interscience: New York, 1971; Chapter 3.
(3) Tolman, C. A. *Chem. Rev.* **1977**, *77*, 313.
(4) Benfield, R. E.; Johnson, B. F. G. *J. Chem. Soc., Dalton Trans.* **1980**, 1743.
(5) Doedens, R. J.; Dahl, L. F. *J. Am. Chem. Soc.* **1966**, *88*, 4847.
(6) Mingos, D. M. P. *Inorg. Chem.* **1982**, *21*, 464.
(7) Mansassero, M.; Sansoni, M.; Longoni, G. *J. Chem. Soc., Chem. Commun.* **1976**, 919.
(8) Muetterties, E. L.; Stein, J. *Chem. Rev.* **1979**, *79*, 479.
(9) (a) Whitmire, K. H.; Shriver, D. F. *J. Am. Chem. Soc.* **1981**, *103*, 6754. (b) Whitmire, K.; Shriver, D. F. *Ibid.* **1980**, *102*, 1456.
(10) Drezdzon, M. A.; Whitmire, K. H.; Bhattacharyya, A. A.; Hsu, W.-L.; Nagel, C. C.; Shore, S. G.; Shriver, D. F. *J. Am. Chem. Soc.* **1982**, *104*, 5630.

0020-1669/84/1323-2491$01.50/0

complexes. As described above these might undergo M–M bond scission due to steric crowding and adopt a butterfly geometry with η^2-CO, analogous to that of II. High-yield syntheses were devised for $[Fe_3M(CO)_{14}]^{2-}$, but the nature of the distortion resulting from steric crowding of the CO ligands is not as anticipated. These observations prompted modeling studies of the strain energies in $M_4(CO)_{14}$ species.

Experimental Section

Materials and Methods. All manipulations were performed under an atmosphere of prepurified N_2 by using standard Schlenk techniques. THF and $(i\text{-Pr})_2O$ were dried over sodium benzophenone ketyl, and CH_2Cl_2 was dried over P_2O_5. All solvents were freshly distilled prior to use and deaerated with N_2. CH_3CN was deaerated with N_2 before being used.

$Cr(CO)_6$, $Mo(CO)_6$, and $W(CO)_6$ (Strem Chemicals) were used without further purification as was $(CH_3)_3OBF_4$ (Alfa Products). CH_3SO_3F (Aldrich), HSO_3CF_3 (Aldrich), and $CF_3C(O)OH$ (MCB) were vacuum distilled for purification. $Cr(CO)_3(CH_3CN)_3$, $Mo(CO)_3(CH_3CN)_3$, and $W(CO)_3(CH_3CN)_3$ were prepared by literature procedures,[11] and the purity was determined by infrared spectroscopy.[12] The $Fe_3(CO)_{12}$[13] used in the preparation of $[PPN]_2[Fe_3(CO)_{11}]$[14] (PPN = bis(triphenylphosphine)nitrogen(1+)) was kindly supplied by M. A. Drezdzon.

NMR spectra were obtained on a JEOL FX-270 spectrometer (^1H, 269.65 MHz; ^{13}C, 67.80 MHz). All spectra were obtained in CD_2Cl_2 (99.5 atom %), which was dried over P_2O_5 and vacuum distilled prior to use. Infrared spectra were recorded on either a Model 283 or 399 Perkin-Elmer spectrophotometer. Solution cells with 0.1-mm path lengths and CaF_2 windows were used.

Synthesis of $[PPN]_2[Fe_3M(CO)_{14}]$ (M = Cr, Mo, W). The synthesis of the three clusters is essentially identical. Under an inert atmosphere, 1 equiv of $Cr(CO)_3(CH_3CN)_3$ was added slowly while stirring to 1.0 g of $[PPN]_2[Fe_3(CO)_{11}]$ dissolved in 15 mL of CH_2Cl_2. After 30 min the solution was filtered through a medium-porosity frit, the solvent removed under vacuum, and the solid dried under vacuum. This solid was redissolved in THF, filtered, and recovered by stripping the solvent under vacuum. It was then recrystallized from CH_2Cl_2/isopropyl ether and washed with hexane, to produce $[PPN]_2[Fe_3Cr(CO)_{14}]$ in 85% yield. The solids were all isolated as black crystalline air-sensitive materials. Anal. Calcd for $Fe_3CrC_{86}H_{60}O_{14}P_4N_2$: Fe, 9.93; Cr, 3.08; N, 1.66. Found: Fe, 10.59; Cr, 3.09; N, 1.68. Anal. Calcd for $Fe_3MoC_{86}H_{60}O_{14}P_4N_2$: N, 1.62; Fe, 9.67; Mo, 5.54. Found: N, 1.63; Fe, 8.23; Mo, 4.08. Anal. Calcd for $Fe_3WC_{86}H_{60}O_{14}P_4N_2$: C, 56.69, H, 3.29; N, 1.53; W, 10.09; Fe, 9.20. Found: C, 54.78; H, 3.69; N, 1.47; W, 8.83; Fe, 8.68.

Reaction of $[PPN]_2[Fe_3M(CO)_{14}]$ with Acid. A 1-equiv portion of either $CF_3C(O)OH$ or CF_3SO_3H was added to a solution containing 250 mg of the appropriate cluster in 10 mL of CH_2Cl_2 at −78 °C. Warming the mixture to room temperature caused decomposition. Infrared spectroscopy was used to identify the decomposition products.

Alkylation of $[PPN]_2[Fe_3M(CO)_{14}]$ with CH_3^+. Experimental procedures were similar for all clusters except CH_3SO_3F replaces $(CH_3)_3OBF_4$ for M = Cr. A 2.0-equiv sample of CH_3SO_3F was added under a N_2 atmosphere to 1.0 g of $[PPN]_2[Fe_3Cr(CO)_{14}]$ in 10 mL of CH_2Cl_2. After reaction was complete (10 min), the solution was filtered through a medium-porosity frit, the solvent removed under vacuum, and the solid dried under vacuum. Isopropyl ether was used to redissolve the solid and the $(PPN)SO_3F$ ($(PPN)BF_4$) removed by filtration. The ether volume was reduced until crystals formed, and these were collected; yield 50%. No similar crystalline product could be obtained for M = Mo or W. Analysis of the chromium product showed it to be $[PPN][Fe_3(CO)_{10}(COMe)]$. Anal. Calcd for $Fe_3C_{47}H_{63}O_{11}P_2N$: N, 1.38; Fe, 16.51. Found: N, 1.31; Fe, 16.54 [Cr, 0.28].

Successive Alkylation and Protonation. To the crystalline product, M = Cr, or crude material, M = W, in CH_2Cl_2 was added 1 equiv of CF_3SO_3H at −78 °C. For M = Cr a product was isolated, from hexane, and characterized as $HFe_3(CO)_{10}(COMe)$ by IR and ^1H NMR spectroscopy. When M = W, no isolable compound was obtained.

Single-Crystal X-ray Structure Determination. A crystal of $[N(PPh_3)_2]_2[Fe_3Cr(CO)_{14}]$ was sealed in a capillary and mounted on a Syntex P_3 automated diffractometer. Unit cell dimensions (Table I) were determined by least-squares refinement of the best angular positions for 15 independent reflections ($2\theta > 15°$) during normal alignment procedures using molybdenum radiation (λ = 0.71069 Å). Data (17040 points) were collected at room temperature by using a variable scan rate, a θ–2θ scan mode, and a scan width of 1.2° below $K\alpha_1$ and 1.2° above $K\alpha_2$ to a maximum 2θ value of 116°. Backgrounds were measured at each side of the scan for a combined time equal to the total scan time. The intensities of three standard reflections were remeasured after every 97 reflections, and for the intensities of these reflections showing less than 8% variation, corrections for decomposition were deemed unnecessary. Data were corrected for Lorentz, polarization, and background effects but not for extinction. After removal of redundant and space group forbidden data, 5074 reflections were considered observed [$I > 3.0\,\sigma(I)$]. The structure was solved by direct methods using MULTAN80.[15] Refinement of scale factor, positional, and anisotropic thermal parameters[16] for all nonhydrogen atoms was carried out to convergence. Hydrogen positional parameters were not determined. The final cycle of refinement [function minimized $\sum(|F_o| - |F_c|)^2$] led to a final agreement factor, R = 8.5%, [$R = 100(\sum||F_o| - |F_c||/|F_o|)$]. Anomalous dispersion corrections were made for Fe and Cr. Scattering factors were taken from Cromer and Mann.[17] Unit weights were used throughout.

Table I. Crystal Data for $[PPN]_2[Fe_3Cr(CO)_{14}]$

formula	$Fe_3CrC_{86}H_{60}O_{14}P_4N_2$
mol wt	1688.7
habit	irregular chunk
approx cryst dimens, mm	$<(0.5 \times 0.5 \times 0.5)$[a]
a, Å	13.428 (5)
b, Å	17.734 (5)
c, Å	18.254 (9)
α, deg	95.46 (3)
β, deg	105.74 (3)
γ, deg	69.82 (2)
V, Å^3	3927.0 (24)
$F(000)$	1728
μ(Mo Kα)	8.52
λ(Mo Kα), Å	0.71069 Å
monochromator	graphite
D_{calcd}, g cm^{-3}	1.43
Z	2
no. of obsd reflcns	5074
R, %	8.5
space group	$P\bar{1}$
octants measd	$\pm h, k, \pm l$

[a] Sealed in 0.5-mm glass capillary under N_2.

Results and Discussion

Mixed-Metal Cluster Formation. The reaction of $[PPN]_2[Fe_3(CO)_{11}]$ with a labile group 6B reagent is complete in less than 5 min and is accompanied by a color change from the orange-brown characteristic of $[Fe_3(CO)_{11}]^{2-}$ to brown-black. It is important to note that reaction 2 does not proceed

$$[PPN]_2[Fe_3(CO)_{11}] + M(CO)_3(CH_3CN)_3 \xrightarrow{CH_2Cl_2} [PPN]_2[Fe_3M(CO)_{14}] + 3CH_3CN \quad (2)$$

to an appreciable extent in coordinating solvents such as tetrahydrofuran (THF) and acetonitrile. The parent cluster, $[Fe_3(CO)_{11}]^{2-}$, possesses a bridging carbonyl band in CH_2Cl_2 at 1670 cm^{-1},[18] which disappears upon product formation. By

(11) Tate, D. P.; Knipple, W. R.; Augl, J. M. *Inorg. Chem.* **1962**, *1*, 433.
(12) Ross, B. L.; Grasselli, J. G.; Ritchey, W. M.; Kaesz, H. D. *Inorg. Chem.* **1963**, *2*, 1023.
(13) McFarlane, W.; Wilkinson, G. *Inorg. Synth.* **1966**, *8*, 181.
(14) Hodali, H. A.; Shriver, D. F. *Inorg. Synth.* **1980**, *20*, 218.
(15) Main, P.; Fiske, S. J.; Hull, S. E.; Lessinger, L.; Germain, G.; DeClerq, J. P.; Woolfson, M. M. "Multan 80"; University of York: York England, 1980.
(16) Stewart, J. M., Ed. "The X-RAY System", Version of Technical Report TR446; Computer Center, University of Maryland: College Park, MD, 1980.
(17) Cromer, D. T.; Mann, T. B. *Acta Crystallogr., Sect. A* **1968**, *A24*, 321.
(18) Butts, S. B.; Shriver, D. F. *J. Organomet. Chem.* **1979**, *169*, 191.

Table II. Infrared Stretching Frequencies[a]

compd	ν_{CO}(terminal), cm^{-1}	ν_{CO}(bridging), cm^{-1}
$[PPN]_2[Fe_3Cr(CO)_{14}]$	1950 vs, br; 1915 m, sh; 1860 w, sh	1760 vw, br
$[PPN]_2[Fe_3Mo(CO)_{14}]$	1980 s, sh; 1948 vs; 1906 m, sh; 1864 w, sh	1775 vw, br
$[PPN]_2[Fe_3W(CO)_{14}]$	1960 s, sh; 1940 vs; 1905 m; 1862 w	1750 vw, br
$[PPN][Fe_3Cr(CO)_{13}(COMe)]$	1983 vs; 1945 m, sh; 1870 vw	
$[PPN][Fe_3Mo(CO)_{13}(COMe)]$	1985 vs; 1950 sh	
$[PPN][Fe_3W(CO)_{13}(COMe)]$	1980 vs, br; 1942 m, sh	

[a] CH_2Cl_2 solution.

controlled addition of the $M(CO)_3(CH_3CN)_3$ reagent and concurrent monitoring of the 1670-cm^{-1} absorption band, the stoichiometry of the reaction can be shown to be 1:1 $[Fe_3(CO)_{11}]^{2-}$:$M(CO)_3(CH_3CN)_3$. If excess $M(CO)_3L_3$ is added, the absorptions due to this species[12] are observed in the infrared spectrum, suggesting that no higher nuclearity clusters are formed.

The CO stretching frequencies for IIIa–c in CH_2Cl_2 (Table II) are similar for all three compounds, suggesting that they are likely to be isostructural. The salient features of the spectra are the appearance of an absorption at ~1750 cm^{-1}, characteristic of an edge-bridging carbonyl, and the lack of absorptions between 1300 and 1700 cm^{-1}. Most of the known η^2-carbonyls display absorptions in this latter region (Table III). No specific absorption has been assigned to the η^2-CO in $[HFe_4(CO)_{13}]^-$, but it seems likely that it would fall in a region below that of the other η^2-carbonyls because of the increased back-bonding to the CO due to the overall negative charge on the molecule.

The compounds were further characterized by variable-temperature ^{13}C NMR spectroscopy (Table IV). The NMR spectrum of the η^2-CO in the two tetranuclear clusters that are known to contain this ligand exhibits a large downfield shift from the terminal CO region, δ 279.7 and 281.4 for $[HFe_4(CO)_{13}]^-$ and $Cp_2Cp_2'Co_2Mo_2(CO)_4$,[19j] respectively. The binuclear complexes containing η^2-CO generally display resonances only in the terminal CO region.[19a-h]

Both the chromium and molybdenum compounds, IIIa and b, possess downfield resonances, δ 291.4 and 289.3 at −90 °C, respectively. $[Fe_3W(CO)_{14}]^{2-}$ displays a single resonance at δ 222.2 down to −90 °C. Although these resonances for $[Fe_3Cr(CO)_{14}]^{2-}$ and $[Fe_3Mo(CO)_{14}]^{2-}$ are similar to those for the η^2-CO compounds previously mentioned, they are also in the range for some edge-bridging carbonyls. In $[HFe_3(CO)_{11}]^-$ for example, the edge-bridging CO appears at δ 284.0[20] and the bridging carbonyls in the mixed cobalt–molybdenum compound mentioned above appear at δ 294.1. Warming both $[Fe_3Cr(CO)_{14}]^{2-}$ and $[Fe_3Mo(CO)_{14}]^{2-}$ to ca. 30 °C causes collapse of the downfield resonance and ultimately complete equivalence of the carbonyls. Figure 1 contains the ^{13}C NMR spectrum of the molybdenum derivative at different temperatures. In summary, the NMR data are consistent with the presence of η^2-CO in these systems, but they do not prove the presence of this structural feature. This structural ambiguity led to an X-ray structure determination that demonstrates the absence of an η^2-CO in $[Fe_3Cr(CO)_{14}]^{2-}$; see below.

Table III. Infrared Spectra of η^2-CO Species

compd	$\nu_{\eta^2\text{-CO}}$, cm^{-1}	ref
$Mn_2(CO)_5(dppm)_2$[a]	1648	19a
$Mn_2(CO)_5(depm)_2$[b]	1640	19b
$Mn_2(CO)_5(dcpm)_2$[c]	1646	19b
$CpCo(CO)_2ZrCp_2'$[d,e]	1683	19c
$Cp_3TiW(\mu\text{-CR})(CO)_2$[f]	1638	19d
$Cp_3ZrW(\mu\text{-CR})(CO)_2$[f]	1578	19d
$Cp_3NbMo(CO)_3$	1560	19e
$Cp_3ZrMo(CO)_3(\mu\text{-}CH_3CO)$	1534	19f, g
$Cp_2MoW_2(\mu\text{-CR})_2(CO)_6$[f]	1687	19h
$Cp_3Nb_3(CO)_7$	1330	19i
$Cp_2Cp_2'Co_2Mo_2(CO)_4$	1633	19j

[a] dppm = $Ph_2PCH_2PPh_2$. [b] depm = $Et_2PCH_2PPh_2$. [c] dcpm = $(c\text{-}C_6H_{11})_2PCH_2PPh_2$. [d] Cp = $\eta\text{-}C_5H_5$. [e] Cp' = $\eta\text{-}Me_5C_5$. [f] R = $C_6H_4Me\text{-}4$.

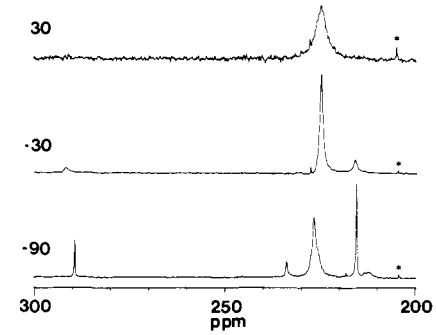

Figure 1. Variable-temperature ^{13}C NMR spectra of $[Fe_3Mo(CO)_{14}]^{2-}$. Resonance marked with an asterisk is $Mo(CO)_6$ impurity.

Reaction with H^+. With the thought that both steric crowding and protonation of the metal framework may be responsible for the structural transformation in eq 1, we investigated the protonation of the mixed-metal clusters. Low-temperature, −78 °C, protonations were performed on $[Fe_3Cr(CO)_{14}]^{2-}$, $[Fe_3Mo(CO)_{14}]^{2-}$, and $[Fe_3W(CO)_{14}]^{2-}$ with either $CF_3C(O)OH$ or HSO_3CF_3. The protonated chromium and molybdenum complexes are unstable above −50 °C as evidenced by a rapid color change from brown-black to red-purple followed, in the case of the molybdenum cluster, by a further change to green. Infrared spectra show the red-purple solution to be $[HFe_3(CO)_{11}]^-$ and the green solution to be $Fe_3(CO)_{12}$. The conversion of $[HFe_3(CO)_{11}]^-$ in acidic solutions to $Fe_3(CO)_{12}$ is the method often employed to synthesize the latter.[13] The fate of the molybdenum in this reaction is unknown. The stability of the tungsten analogue proved to be greater than for the molybdenum. The solution could be warmed to room temperature and maintained at this temperature for short periods of time before decomposition occurred. The complex is sufficiently stable to permit the determination of its infrared spectrum, which shows a broad single absorption centered at 2000 cm^{-1}. No bridging bands

(19) (a) Colton, R.; Commons, C. J.; Hoskins, B. F. *J. Chem. Soc., Chem. Commun.* **1975**, 363. (b) Wolff, T. E.; Klemann, L. P. *Organometallics* **1982**, *1*, 1667. (c) Barger, P. T.; Bercaw, J. E. *J. Organomet. Chem.* **1980**, *201*, C39. (d) Dawkins, G. M.; Green, M.; Mead, K. A.; Salaiin, J.-Y.; Stone, F. G. A.; Woodward, P. *J. Chem. Soc., Dalton Trans* **1983**, 527. (e) Pasynskii, A. A.; Skripkin, Yu. V.; Eremenko, I. L.; Kallinikov, V. T.; Aleksandrov, G. G.; Andrianov, V. G.; Struckov, Yu. T. *J. Organomet. Chem.* **1979**, *165*, 49. (f) Marsella, J. A.; Huffman, J. C.; Caulton, K. G.; Longato, B.; Norton, J. R. *J. Am. Chem. Soc.* **1982**, *104*, 6360. (g) Longato, B.; Norton, J. R.; Huffman, J. C.; Marsella, J. A.; Caulton, K. G. *Ibid.* **1981**, *103*, 209. (h) Carriedo, G. A.; Hodgson, D.; Howard, J. A. K.; Marsden, K.; Stone, F. G. A.; Went, M. J.; Woodward, P. *J. Chem. Soc., Chem. Commun.* **1982**, 1006. (i) Herrmann, W. A.; Ziegler, M. L.; Weidenhammer, K.; Biersack, H. *Angew. Chem., Int. Ed. Engl.* **1979**, *18*, 960. (j) Brun, P.; Dawkins, G. M.; Green, M.; Miles, A. D.; Orpen, A. G.; Stone, F. G. A. *J. Chem. Soc., Chem. Commun.* **1982**, 926.

(20) Wilkinson, J. R.; Todd, L. J. *J. Organomet. Chem.* **1976**, *118*, 199.

Table IV. ^{13}C NMR Chemical Shifts[a]

compd	−90 °C	−50 °C	−30 °C	+30 °C
$[PPN]_2[Fe_3Cr(CO)_{14}]$	291.4, 229.7, 216.1, 215.8, 213.7, 210.5	293.6, 229.7, 216.3, 210.6		229.5
$[PPN]_2[Fe_3Mo(CO)_{14}]$	289.3, 233.7, 226.4, 215.3		292.8, 228.2, 225.4, 216.5	225.9
$[PPN]_2[Fe_3W(CO)_{14}]$	222.2			222.7

[a] All values in ppm relative to external Me_4Si.

are observed. The final decomposition product displays no carbonyl bands and thus must follow a different decomposition path than that of the molybdenum derivative.

In order to obtain NMR spectral data on these protonated compounds, in situ protonations were performed at −78 °C in NMR tubes with $CF_3C(O)OH$ and NMR spectra were obtained immediately at −90 °C. Protonation of $[Fe_3Cr(CO)_{14}]^{2-}$ causes appearance of a single resonance in the ^1H NMR spectrum at δ −21.6, a value typical for a metal hydride. The ^1H spectrum of $[HFe_3Mo(CO)_{14}]^-$ displays two upfield resonances, δ −15.4 and −17.6. This result suggests that protonation occurs across a metal–metal bond and that two isomers may exist. The tungsten compound shows a single upfield resonance at δ −14.8, again consistent with protonation across a metal–metal bond. The low-temperature ^{13}C NMR spectrum of $[HFe_3Cr(CO)_{14}]^{2-}$ displays two resonances, δ 229.3 and 216.2. The latter resonance may be due to $[HFe_3(CO)_{11}]^-$,[20] but the important feature of the spectrum is the lack of any downfield resonances. Warming this compound to −20 °C causes an upfield shift of the single resonance to δ 223.6. Higher temperatures were not investigated due to the decomposition previously mentioned. The ^{13}C NMR spectrum of $[HFe_3Mo(CO)_{14}]^-$ is complicated by resonances due to starting material as well as product. However, the new resonances appeared only in the region typical for terminally bound carbonyls. The lack of additional downfield resonances suggests that a butterfly compound analogous to II is not the product of protonation. Similarly for $[HFe_3W(CO)_{14}]^-$ no downfield resonances are observed in the ^{13}C NMR spectrum. Only a single resonance similar to the parent dianion is observed at δ 222.5 at −90 °C. This resonance shifts to δ 216 at 0 °C. In summary, we find no NMR evidence for η^2-CO in the series of $[HFe_3M(CO)_{14}]^-$ clusters, so it appears that a structural transformation similar to that in eq 1 has not taken place.

Reactions with CH_3^+. Each of the dianionic clusters was allowed to react with a strong carbocation reagent, CH_3SO_3F for $[Fe_3Cr(CO)_{14}]^{2-}$ and $(CH_3)_3OBF_4$ for both $[Fe_3W(CO)_{14}]^{2-}$ and $[Fe_3Mo(CO)_{14}]^{2-}$. The infrared stretching frequencies for these alkylation products are listed in Table II. As in the case of the dianions the infrared spectra for the three compounds are essentially identical. However, the cluster initially containing chromium was subsequently shown by elemental analysis as well as protonation of the isolated product to no longer contain this element. The cluster isolated from the alkylation reaction is $[Fe_3(CO)_{10}(COMe)]^-$. Furthermore, the ^1H NMR spectrum of the protonated species agreed well with literature values for $HFe_3(CO)_{10}(COMe)$.[21] Thus, the methylation reaction of $[Fe_3Cr(CO)_{14}]^{2-}$ seems to parallel the reaction seen for the protonation of $[Fe_3Mo(CO)_{14}]^{2-}$ where the heterometal has been cleaved from the cluster framework. Similar decomposition reactions have been observed in other mixed-metal systems where the final product clusters contain only one metal species.[22]

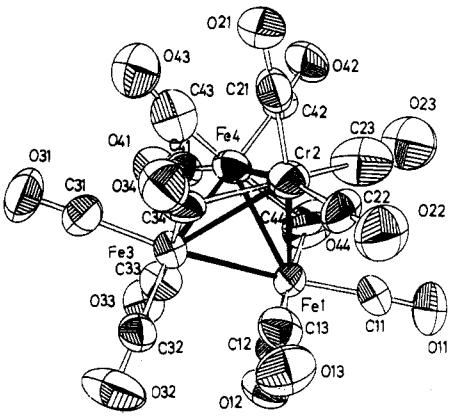

Figure 2. ORTEP diagram of $[Fe_3Cr(CO)_{14}]^{2-}$ showing 50% probability thermal ellipsoids and the atom-numbering scheme.

Despite the apparently similar structures indicated by IR spectroscopy of the three alkylated species, they display different solubility properties. Both the molybdenum and tungsten derivatives are only slightly soluble in ether whereas $[Fe_3(CO)_{10}(COMe)]^-$ is quite soluble in this solvent. These results suggested the possibility that the metal framework retained its original composition upon methylation. Unfortunately, no pure crystalline product could be isolated for either species. The tungsten derivative was allowed to react with HSO_3CF_3 at −78 °C. A species similar to $HFe_4(CO)_{12}(COMe)$ (IV), which contains an η^2-$COCH_3$ ligand,[23,24] might

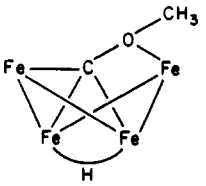

IV

potentially arise from this reaction. However, protonation of $[FeW(CO)_{13}(COMe)]^-$ proved to be a complicated reaction. The infrared spectrum in the carbonyl region shifts about 50 cm^{-1} to higher frequency, consistent with formation of a neutral product. However, the product is insoluble in aliphatic and aromatic solvents and appears to react with coordinating solvents such as ethers and CH_3CN. The reaction with these solvents was not a deprotonation reaction to re-form the methylated product, as evidenced by comparison of infrared spectra. No crystalline product could be isolated on a consistent basis from this reaction.

X-ray Structure of $[Fe_3Cr(CO)_{14}]^{2-}$. The structure of the compound was investigated by single-crystal X-ray diffraction techniques to determine the presence of edge-bridging or η^2-carbonyl groups and to evaluate the structural consequences of the presence of 14 carbonyl ligands in a tetranuclear cluster. The molecular structure of $[Fe_3Cr(CO)_{14}]^{2-}$ is shown in Figure

(21) (a) Shriver, D. F.; Lehman, D.; Strope, D. *J. Am. Chem. Soc.* **1975**, *97*, 1594. (b) Hodali, H. A.; Shriver, D. F. *Inorg. Chem.* **1979**, *18*, 1236.

(22) Steinhardt, P. C.; Gladfelter, W. L.; Harley, A. D.; Fox, J. R.; Geoffroy, G. L. *Inorg. Chem.* **1980**, *19*, 332.

(23) (a) Holt, E. M.; Whitmire, K. H.; Shriver, D. F. *J. Chem. Soc., Chem. Commun.* **1980**, 780. (b) Dawson, P. A.; Johnson, B. F. G.; Lewis, J.; Raithby, P. R. *Ibid.* **1980**, 781.

(24) Holt, E. M.; Whitmire, K. H.; Shriver, D. F. *J. Organomet. Chem.* **1981**, *213*, 125.

Table V. Positional Parameters for $[PPN]_2[Fe_3Cr(CO)_{14}]$[a]

atom	x	y	z
Fe1	−0.0230 (2)	0.2019 (1)	0.8161 (1)
Cr2	0.0572 (2)	0.2416 (2)	0.7169 (2)
Fe3	−0.0510 (2)	0.3561 (1)	0.8013 (1)
Fe4	−0.1560 (2)	0.2806 (2)	0.6910 (1)
O11	0.1017 (20)	0.0300 (9)	0.8301 (11)
O12	−0.1082 (13)	0.1930 (8)	0.9442 (7)
O13	0.1757 (11)	0.2286 (10)	0.9165 (8)
O21	0.0621 (13)	0.3042 (8)	0.5771 (7)
O22	0.2921 (12)	0.1714 (9)	0.7751 (8)
O23	0.0451 (15)	0.0872 (9)	0.6504 (9)
O31	−0.1617 (12)	0.5276 (7)	0.7611 (8)
O32	0.0514 (14)	0.4067 (9)	0.9543 (7)
O33	−0.2410 (10)	0.3601 (7)	0.8563 (7)
O34	0.1254 (11)	0.3934 (8)	0.7544 (8)
O41	−0.3889 (11)	0.3566 (9)	0.6848 (8)
O42	−0.1970 (15)	0.1937 (10)	0.5468 (8)
O43	−0.1670 (12)	0.4189 (9)	0.6094 (9)
O44	−0.2027 (16)	0.1377 (10)	0.7320 (9)
C11	0.0525 (20)	0.0988 (13)	0.8239 (11)
C12	−0.0780 (15)	0.1992 (10)	0.8941 (9)
C13	0.0923 (15)	0.2290 (12)	0.8715 (11)
C21	0.0586 (15)	0.2774 (10)	0.6320 (10)
C22	0.1971 (16)	0.2015 (11)	0.7520 (11)
C23	0.0431 (20)	0.1511 (16)	0.6825 (14)
C31	−0.1198 (15)	0.4601 (10)	0.7759 (10)
C32	0.0122 (15)	0.3860 (10)	0.8940 (9)
C33	−0.1671 (15)	0.3487 (11)	0.8305 (10)
C34	0.0683 (14)	0.3614 (11)	0.7622 (9)
C41	−0.2972 (16)	0.3269 (11)	0.6874 (10)
C42	−0.1755 (17)	0.2256 (11)	0.6049 (10)
C43	−0.1529 (15)	0.3653 (12)	0.6515 (13)
C44	−0.1506 (18)	0.1793 (12)	0.7441 (10)

[a] Errors in least significant digits given in parentheses.

2. Final positional parameters are given in Table V. Derived distances and angles are listed in Table VI. $[PPN]_2[Fe_3Cr(CO)_{14}]$ crystallizes in a centrosymmetric triclinic space group with one dianionic metal tetramer and two bis(triphenylphosphine)nitrogen(1+) cations per asymmetric unit. The 60-electron cluster displays a pseudotetrahedral arrangement of metal atoms with only small distortions that may be attributed to its heterometal composition. Four refinements were performed in which the chromium was placed at each of the vertices. Comparisons between U_{equiv} were made for each of the refinement cycles. U_{equiv} is the average of U_{11}, U_{22}, and U_{33} for each atom, and when correct positional assignments are made, the value of U_{equiv} at each position should be nearly the same. A table of U_{equiv} (Table VII) shows that in the reported refinement the U_{equiv} range from 0.0488 to 0.0574 while for the next most reasonable refinement a difference of 0.019 exists between U_{equiv}. The evidence for the preferred metal array is not strong, but we shall use this ordered array to facilitate subsequent discussion of the structure.

The three Fe–Cr distances (average 2.633 (25) Å) are slightly shorter than the Fe–Fe distances (average 2.655 (4) Å). Each metal binds to three terminal carbonyl groups [Fe–$C_{terminal}$(av) = 1.78 (2) Å, Cr–$C_{terminal}$(av) = 1.73 (2) Å]. Within the three Fe–Cr distances, the two nonbridged bonds Fe1–Cr2 and Fe4–Cr2 are significantly shorter than the asymmetrically bridged bond, Fe3–Cr2. Formal electron-counting rules would suggest that Cr2 is electron deficient and the irons are electron rich. One of the terminal carbonyl groups bonded to each of the four metal atoms may be characterized as "slightly bent" (metal–C–O = 163.4 (19)–168.6 (26)°) as compared to the 174.5 (17)–179.7 (25)° average observed for the other terminal carbonyl groups at each metal atom. Fe1 and Fe4 are bridged by carbonyl group C44–O44 (Fe1–C44 = 1.99 (2) Å, Fe4–C44 = 2.09 (2) Å, Fe1–C44–O44 = 144.4 (16)°, Fe4–C44–O44 = 134.7 (14)°), while Cr2 and Fe3 are bridged in less symmetrical fashion by carbonyl C34–O34 (Fe3–C34 = 1.95 (2) Å, Cr2–C34 = 2.24 (2) Å, Fe3–C34–O34 = 152.1 (14)°, Cr2–C34–O34 = 128.8 (14)°). It is noteworthy that the shortening of the metal–metal bond bridged by a carbonyl observed in other cluster systems is not evident here.

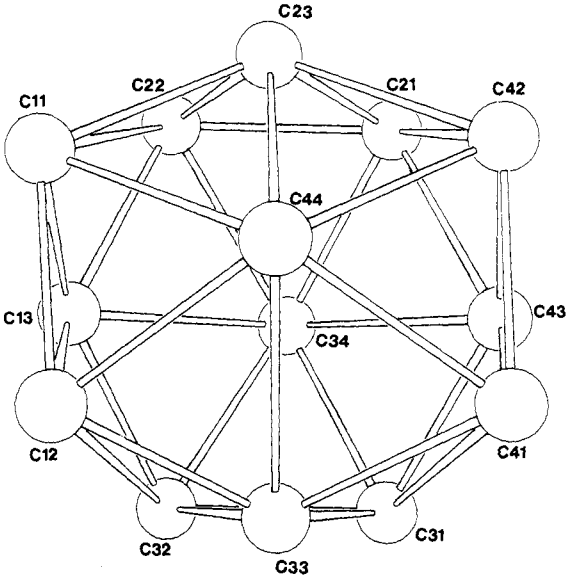

Figure 3. Polyhedron of carbonyl carbons as viewed down the approximate twofold axis of $[Fe_3Cr(CO)_{14}]^{2-}$.

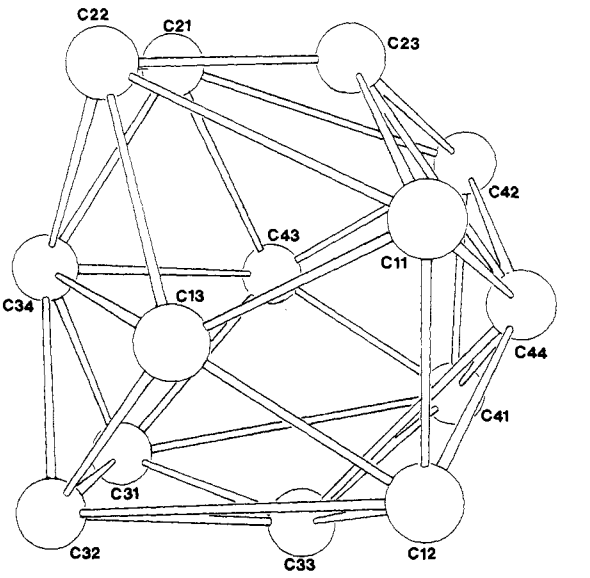

Figure 4. Side view of carbon polyhedron showing the boat conformation of the six-membered rings of $[Fe_3Cr(CO)_{14}]^{2-}$.

Comparisons may be made with the isoelectronic four-iron cluster,[5] $[Fe_4(CO)_{13}]^{2-}$ (I), which may be characterized as a tetrahedron of metal atoms, three members of which form a basal plane. In this cluster the Fe–Fe distances are uniformly shorter [Fe_{basal}–Fe_{basal}(av) = 2.50 Å, Fe_{apical}–Fe_{basal}(av) = 2.58 Å] than in the title structure, and the edge-bridging carbonyl groups are bonded to one basal iron atom (Fe_{basal}–$C_{bridging}$ = 1.80, 1.81, 1.85 Å) while being closely attracted to a second iron atom (Fe_{basal}···$C_{bridging}$ = 2.24, 2.28, 2.33 Å), details that are similar to those involving C34 in the title structure.

The disposition of the carbonyl carbon atoms is shown in Figures 3 and 4. The view in Figure 3 is down the approximate twofold axis defined by the bridging carbonyl carbons C44 and C34. In this view the twofold axis passes through C44, the midpoint of the Fe1–Fe4 bond, the midpoint of the Cr2–Fe3 bond, and C34. Approximately perpendicular to this axis are two six-membered carbon rings, staggered relative to

Table VI. Bond Distances (Å) and Angles (deg) for $[PPN]_2[Fe_3Cr(CO)_{14}]$

Fe1-Cr2	2.598 (5)	Cr2-Fe1-Fe3	61.3 (1)
Fe1-Fe3	2.657 (4)	Cr2-Fe1-Fe4	59.9 (1)
Fe1-Fe4	2.650 (4)	Fe3-Fe1-Fe4	60.2 (1)
Cr2-Fe3	2.681 (4)	Fe1-Cr2-Fe3	60.4 (1)
Cr2-Fe4	2.619 (4)	Fe1-Cr2-Fe4	61.0 (1)
Fe3-Fe4	2.660 (4)	Fe3-Cr2-Fe4	60.2 (1)
Fe1-C11	1.77 (2)	Fe1-Fe3-Cr2	58.2 (1)
Fe1-C12	1.78 (2)	Fe1-Fe3-Fe4	59.8 (1)
Fe1-C13	1.79 (2)	Cr2-Fe3-Fe4	58.7 (1)
Fe1-C44	1.99 (2)	Fe1-Fe4-Cr2	59.1 (1)
Cr2-C21	1.74 (2)	Fe1-Fe4-Fe3	60.1 (1)
Cr2-C22	1.72 (2)	Cr2-Fe4-Fe3	61.0 (1)
Cr2-C23	1.72 (3)	Fe1-C11-O11	177.8 (26)
Cr2-C34	2.24 (2)	Fe1-C12-O12	175.9 (14)
Fe3-C31	1.80 (2)	Fe1-C13-O13	163.4 (19)
Fe3-C32	1.80 (2)	Fe1-C44-O44	144.4 (16)
Fe3-C33	1.83 (2)	Cr2-C21-O21	176.4 (17)
Fe3-C34	1.95 (2)	Cr2-C22-O22	177.5 (20)
Fe4-C41	1.77 (2)	Cr2-C23-O23	168.6 (26)
Fe4-C42	1.78 (2)	Cr2-C34-O34	128.8 (14)
Fe4-C43	1.74 (2)	Fe3-C31-O31	178.0 (16)
Fe4-C44	2.09 (2)	Fe3-C32-O32	178.7 (18)
C11-O11	1.17 (2)	Fe3-C33-O33	165.0 (16)
C12-O12	1.12 (3)	Fe3-C34-O34	152.1 (14)
C13-O13	1.19 (2)	Fe4-C41-O41	179.7 (25)
C21-O21	1.17 (2)	Fe4-C42-O42	174.5 (17)
C22-O22	1.17 (2)	Fe4-C43-O43	164.7 (18)
C23-O23	1.22 (3)	Fe4-C44-O44	134.7 (14)
C31-O31	1.16 (2)		
C32-O32	1.17 (2)		
C33-O33	1.16 (3)		
C34-O34	1.14 (3)		
C41-O41	1.15 (2)		
C42-O42	1.17 (2)		
C43-O43	1.21 (3)		
C44-O44	1.15 (3)		

each other (C11, C12, C33, C41, C42, C23 (ring A); C13, C32, C31, C43, C21, C22 (ring B)). Inspection of the nonbonded distances (Table VIII) indicates some distances in the ring to be significantly longer than others, but the overall six-membered nature of the ring is apparent.

In a second view, Figure 4, approximately 90° from the view of Figure 3, the bridging carbon atoms are seen at the extreme right and left of the figure and it is apparent that the two six-membered rings occur in interlocking boat conformations. The two axial carbon atoms, C44 and C34, are approximately equidistant from the rectangular planes of their respective boats, differing by only 0.02 Å. The general picture that emerges is that the polyhedron formed by the carbon atoms may be described as a hexacapped rectangular antiprism.

In contrast with this hexacapped rectangular antiprism geometry, the simple repulsive model of Benfield and Johnson[4] indicates that the two energetically most favorable geometries with 14 vertices are the bicapped hexagonal antiprism (Figure 5a) and the omnicapped cube[25] (Figure 5b). The difference in energy is about 3%, with the bicapped hexagonal antiprism lower in energy.[4] The polyhedron of oxygen atoms described by both $[Co_6(CO)_{14}]^{4-}$[26] and $[Co_4Ni_2(CO)_{14}]^{2-}$[27] corresponds closely to the omnicapped cube. It has been suggested[4] that the octahedral metal core of these clusters may govern the resulting polyhedron. For $[HRu_4(CO)_{13}]^-$, the polyhedron (described by H and C) corresponds to a hexacapped rectangular antiprism. This geometry is intermediate between the bicapped hexagonal antiprism and omnicapped cube.[28]

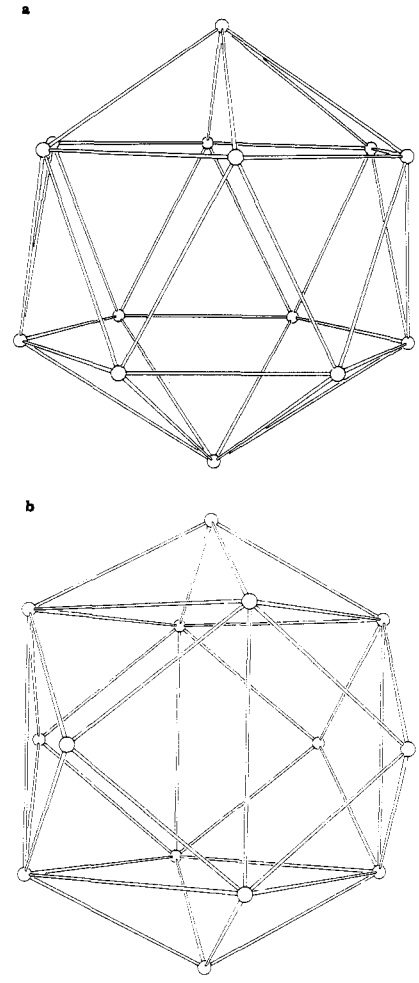

Figure 5. (a) Bicapped hexagonal antiprism. (b) Omnicapped cube.

Interestingly, none of the four molecules mentioned above adopt the calculated lowest energy polyhedron.

Although in most instances the ligand polyhedra have not been described explicitly, there exist a number of isoelectronic metal carbonyl clusters with identical numbers of ligands that show different ligand dispositions. A recent example in which this point was discussed[29] is provided by comparison of $[FeRh_4(CO)_{15}]^{2-}$[29] and $[Rh_5(CO)_{15}]^-$[30] where the metal core geometries are similar but arrangement of the carbonyls differs. (The structure of $[FeRh_4(CO)_{15}]^{2-}$ was inferred from NMR spectral studies.)

Strain Energy. A comparison of the nonbridged Fe–Fe bond distances in $[Fe_4(CO)_{13}]^{2-}$ with those of $[Fe_3Cr(CO)_{14}]^{2-}$ indicates a lengthening on the order of 0.1 Å and a probable increase in M–C distance of about 0.03 Å. Thus, the strain created by the CO–CO repulsions appears to be relieved by a roughly isotropic expansion of the metal tetrahedron (V) accompanied by a modest increase in M–C lengths, rather than the breaking of one M–M bond (VI).

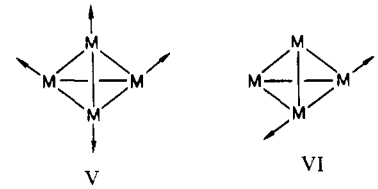

V VI

(25) Casey, J. B.; Evans, W. J.; Powell, W. H. *Inorg. Chem.* **1981**, *20*, 1333.
(26) Albano, V. G.; Bellon, P. L.; Chini, P.; Scattunin, V. *J. Organomet. Chem.* **1969**, *16*, 461.
(27) Albano, V. G.; Ciani, G.; Chini, P. *J. Chem. Soc., Dalton Trans.* **1974**, 432.
(28) Jensen, J. A.; Fjare, D. E.; Gladfelter, W. L. *Inorg. Chem.* **1983**, *22*, 1250.
(29) Additional comparisons are provided in: Ceriotti, A.; Longoni, G.; Pergola, R. D.; Heaton, B. T.; Smith, D. O. *J. Chem. Soc., Dalton Trans.* **1983**, 1433.
(30) Fumagalli, A.; Koetzle, T. F.; Takusagawa, F.; Chini, P.; Martinengo, S.; Heaton, B. T. *J. Am. Chem. Soc.* **1980**, *102*, 1740.

Table VII. U_{equiv} as a Function of Metal Position

	refinement 1		refinement 2		refinement 3		refinement 4	
position	atom no.	U_{equiv}	atom no.	U_{equiv}	atom no.	U_{equiv}	atom no.	U_{equiv}
1	Fe1	0.0581	Cr1	0.0418	Fe1	0.0535	Fe1	0.0543
2	Cr3	0.0382	Fe3	0.0502	Fe3	0.0490	Fe3	0.0494
3	Fe4	0.0602	Fe4	0.0576	Cr4	0.0434	Fe4	0.0574
4	Fe2	0.0620	Fe2	0.0621	Fe2	0.0620	Cr2	0.0488

Table VIII. Nonbonded Carbon-Carbon Distances (Å)

C44-C23	2.99 (4)	C13-C22	2.83 (3)
C44-C11	2.67 (3)	C22-C21	2.61 (2)
C44-C12	2.67 (2)	C21-C43	2.83 (3)
C44-C33	3.23 (3)	C43-C31	2.73 (3)
C44-C41	2.76 (2)	C31-C32	2.51 (2)
C44-C42	2.66 (3)	C32-C13	2.66 (3)
C34-C21	2.68 (2)	C12-C13	2.62 (3)
C34-C43	3.08 (3)	C13-C11	2.58 (3)
C34-C31	2.55 (2)	C11-C22	3.64 (4)
C34-C32	2.66 (3)	C22-C23	2.56 (4)
C34-C13	3.11 (3)	C23-C21	2.62 (4)
C34-C22	2.81 (2)	C21-C42	3.47 (3)
C12-C11	2.54 (3)	C42-C43	2.60 (3)
C11-C23	2.78 (4)	C43-C41	2.48 (4)
C23-C42	2.80 (3)	C41-C31	3.86 (3)
C42-C41	2.64 (3)	C31-C33	2.62 (3)
C41-C33	2.78 (2)	C33-C32	2.64 (3)
C33-C12	2.72 (2)	C32-C12	3.89 (3)

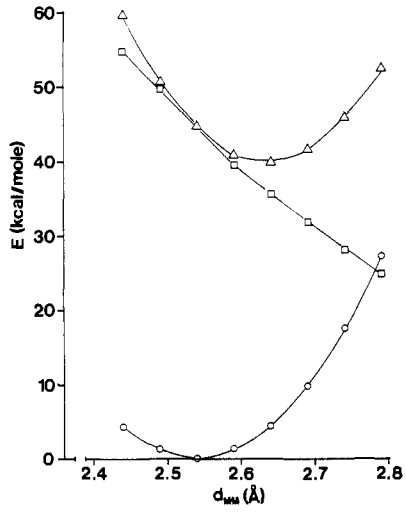

Figure 6. Schematic for energies in strain energy calculation: O (curve 1), sum of the M–M and M–C potentials; □ (curve 2), energy contribution by C–C repulsions; △ (curve 3), total strain energy (sum of curves 1 and 2).

Metal–metal stretching force constants in first-transition-series carbonyls are close to 0.6 mdyn/Å,[31] and M–C force constants are about 2 mdyn/Å.[32] Assuming harmonic potentials, a uniform expansion of the M–M distances by 0.1 Å would require the expenditure of 2.6 kcal/mol and that for a 0.03-Å expansion of M–C would require 1.8 kcal/mol (see Appendix).

The strain energy problem in $M_4(CO)_{14}$ can be described by the evolution of a tetrahedron having normal M–M and M–C bonds but unusually short C–C nonbonding distances to the observed cluster having elongated M–M and M–C bonds and larger more normal C–C nonbonding distances. The relief of C–C repulsive energy is thus offset by increased potential energy in the individual M–M and M–C bonds. The energetics

Table IX. Energy Contributions to Strain Energy in $M_4(CO)_{14}$[a,b]

d_{MM}, Å	E_{MM}	E_{MC}	E_{CC}	E_T
2.79	16.20	11.34	25.09	52.64
2.74	10.37	7.26	28.03	45.93
2.69	5.83	4.08	31.81	44.72
2.64	2.59	1.81	35.65	40.06
2.59	0.65	0.45	39.86	40.96
2.54	0	0	44.48	44.48
2.49	0.65	0.45	49.55	50.65
2.44	2.59	1.81	55.13	59.53

[a] Energies are in kcal/mol. [b] $d_{MM}^0 = 2.54$ Å; $d_0 = 3.4$ Å.

Table X. C–C Distances in Some First-Row Transition-Metal Carbonyl Complexes

	d(C–C), Å	ref	E_{C-C},[a] kcal/mol
$V(CO)_6$[b]	2.83	37	7.77
$[PPN][V(CO)_6]$[b]	2.73	38	11.52
$Cr(CO)_6$[b]	2.71	39	12.43
$Mn_2(CO)_{10}$[b]	2.64 (ax-eq)	40	5.39[e]
	2.58 (eq-eq)		6.73[e]
	3.05 (eq-eq)[d]		1.82
$Ni(CO)_4$[c]	2.99	41	1.90

[a] Calculated for $d_0 = 3.4$ Å in eq 2. [b] X-ray structure. [c] Electron diffraction. [d] This is the distance between the halves of the dimer. [e] These values apply to each half of the dimer.

are illustrated schematically in Figure 6, where the endothermic process of M–M stretching and M–C stretching are combined in one curve and displayed along with a second curve for C–C repulsive energy. These energies are presented as a function of the M–M bond distance, and the method of calculation is described below.

Assuming harmonic potentials, the M–M and M–C energies were evaluated by relatively straightforward procedures described in the Appendix. However the evaluation of the C–C repulsive energy is much less straightforward. The most obvious approach would be to employ a Buckingham potential (eq 3),[33,34] where α is the steepness factor, ϵ the well depth,

$$E_{C-C} = \frac{\epsilon}{1 - 6/\alpha}\left[\frac{6}{\alpha}e^{\alpha(1-(d/d_0))} - \left(\frac{d}{d_0}\right)^6\right] \qquad (3)$$

d_0 the minimum distance, and d the experimental nonbonded distances, which fits C–C repulsions in graphite[35] or organic molecules.[33] The result of using these parameters is an extremely large repulsive energy that could not be reconciled with the energy calculated for the expansion of the M–M distances. Furthermore, use of this unmodified potential yields a large C–C repulsion in $[Fe_4(CO)_{13}]^{2-}$, which appears to be assigned as "strain free" judging from Fe–Fe distances and predicts a structure with an M–M distance of approximately 2.7 Å as most energetically favorable. More realistic energies may be

(31) Onaka, S.; Cooper, C. B., III; Shriver, D. F. *Inorg. Chim. Acta* **1979**, *37*, 2467.
(32) Jones, L. H. "Inorganic Vibrational Spectroscopy"; Marcel Dekker: New York, 1971; p 145.
(33) Engler, E. M.; Andose, J. D.; Schleyer, P. v. R. *J. Am. Chem. Soc.* **1973**, *95*, 8005.
(34) Hirschfelder, J. O.; Curtiss, C. F.; Bird, R. B. "Molecular Theory of Gases and Liquids"; Wiley: New York, 1954.
(35) Coulson, C. A.; Senent, S.; Herraez, M. A.; Leal, M.; Santos, E. *Carbon* **1966**, *3*, 445.

Table XI. Parameters for Strain Energy Calculations[a]

k_{MM}, mdyn/Å	0.6	R_C^0	3.00
k_{MC}, mdyn/Å	2.0	d_{MC}^0	1.72
ϵ	6.6×10^{-4}	R_M^0	1.60
α	12.0	θ, deg	35.65
d_0	3.4	R_C', Å	3.065
d_{MM}^0	2.54		

[a] Calculated quantities were multiplied by 144 to convert them to units of kcal/mol.

obtained by adjusting the value of d_0 from 3.85 Å in the published potential[33] to 3.4 Å. Use of this new d_0 value correctly predicts the M–M distances in the observed structure as the most energetically favorable. The calculated energies using d_0 = 3.4 Å are presented in Table IX.

Comparison of the d_0 value can be made with the interplanar spacing in graphite, 3.35 Å,[36] as well as nonbonded distances in a number of first-row metal carbonyl compounds (Table X). In the case of graphite, the interplanar spacing and the d_0 values are nearly equal; however, in all instances involving the M–CO_x compounds, the d_0 value is larger than the nonbonded contacts. This predicts that all of the metal carbonyls have some degree of strain in them. This strain must obviously be overcome by bonding interactions.

The total strain energy from these calculations, which is the sum of the three individual energy contributions, is shown in Figure 6 (curve 3). The energies are reasonably symmetrically distributed around the minimum, 2.64 Å. As expected, the major contribution to the strain energy in the contracted metal core is due to C–C interactions while both the combined M–M and M–C energies and the C–C repulsions make significant contributions to the total energy at the minimum.

There is significant uncertainty in the value chosen for the unstrained M–M distances, so a range of d_{MM}^0 values was investigated to determine the effect on both E_{total} and d_0. Extreme values chosen in d_{MM}^0 were 2.58 and 2.50 Å. When the procedures outlined above and in the Appendix were utilized, the corresponding d_0 values ranged from 3.2 to 3.6 Å. As expected, the energy minimum was also significantly lower for the larger d_{MM}^0 = 18.5 kcal/mol than for the smaller d_{MM}^0 = 72.2 kcal/mol. It is our impression that the latter is unreasonably high, and we favor the intermediate C–C repulsive parameter d_0 = 3.4 Å. As a further check, total C–C repulsive energies were calculated by using this value of d_0 for simple carbonyls. The results that appear in Table X are chemically reasonable.

The total C–C repulsion energy in $[Fe_3Cr(CO)_4]^{2-}$ at d_{MM} = 2.54 Å is 45 kcal/mol, and this is reduced to 36 kcal/mol by expansion of the metal core to d_{MM} = 2.64 Å. When distributed over the six M–M bonds, the average strain energy per M–M bond, 6 kcal/mol, is significantly less than the average M–M bond energy of ca. 20 kcal/mol.[42] Thus, the energy estimates given here are consistent with the observed stability of the pseudotetrahedral $[M_4(CO)_{14}]^{2-}$ species.

Scheme I

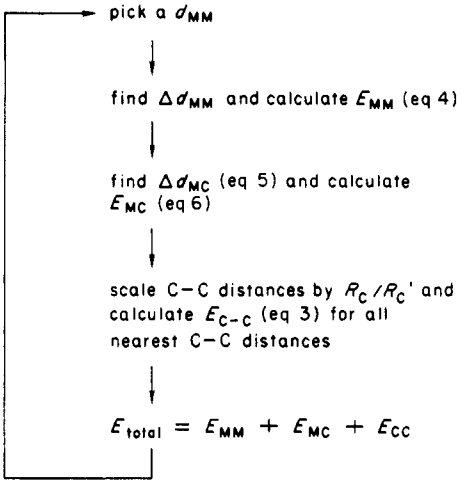

Acknowledgment. This research was funded by NSF Grant CHE-8204401. C.P.H. was the recipient of an E. I. du Pont de Nemours and Co. fellowship. C.P.H. thanks Dr. Paul Swepston for help with the ORFFE program and J. Shriver for the strain program used in strain energy calculations.

Appendix

Since the M–M force constants are small (Table XI), changes in C–C strain energy will be reflected in rather large changes in M–M distances. Also, the M–M distances are known with better accuracy than those between lighter atoms, and the four-metal polyhedron is more symmetrical than the 14-carbon polyhedron. For these reasons the model calculations of strain energy rely heavily on M–M distances. The changes in M–M distances thus become a "strain gauge" by which both the M–C distances and the C–C repulsive parameters are scaled. The metal core is expanded or contracted isotropically, and the total energy for this process is calculated from a harmonic potential (eq 4), where d_{MM}^0 is the unstrained Fe–Fe distance and d_{MM} is the Fe–Fe distance for some arbitrary expansion or contraction of the metal core. The force constant for stretching the Fe–Fe or Fe–Cr bond is k_{MM}.

$$E_{MM} = 3k_{MM}(\Delta d_{MM})^2 \quad \Delta d_{MM} = d_{MM} - d_{MM}^0 \qquad (4)$$

Calculation of E_{MC} is complicated by a number of factors including the various types of CO ligands, i.e., terminal, edge bridging, semibridging, and triply bridging, and the magnitude of experimental errors in M–C distances. In order to simplify the problem, changes in M–C are calculated from eq 5, where

$$\Delta d_{MC} = (k_{MM}/k_{MC})\Delta d_{MM} \qquad (5)$$

k_{MC} is the force constant for the stretching a terminal M–C bond, k_{MM} was defined previously, Δd_{MM} is the change in average M–M distance, and Δd_{MC} is the consequent change in M–C distance. Equation 5 expresses in an average way the fact that the same radial force is exerted on the M–M and M–C bonds. The resulting value for Δd_{MC} permits the calculation of the total M–C potential energy, E_{MC}, as indicated in eq 6.

$$E_{MC} = 7k_{MC}(\Delta d_{MC})^2 \qquad (6)$$

The C–C repulsion energy was calculated by eq 3 using the actual nonbonded distances in $[Fe_3Cr(CO)_{14}]^{2-}$. Changes in C–C distances were calculated by using a scaling factor based on the change in M–M distances and the resulting changes in M–C distances. The function is then reevaluated by using the new C–C distances.

(36) Cotton, F. A.; Wilkinson, G. "Advanced Inorganic Chemistry", 4th ed.; Interscience: New York, 1980.
(37) Bellard, S.; Rubinson, K. A.; Sheldrick, G. M. *Acta Crystallogr., Sect. B* **1979**, *B35*, 271.
(38) Wilson, R. D.; Bau, R. *J. Am. Chem. Soc.* **1974**, *96*, 7601.
(39) Rees, B.; Mitschler, A. *J. Am. Chem. Soc.* **1976**, *98*, 7918.
(40) (a) Churchill, M. R.; Amoh, K. N.; Wasserman, H. J. *Inorg. Chem.* **1981**, *20*, 1609. (b) Dahl, L. F.; Rundle, R. E. *Acta Crystallogr.* **1963**, *16*, 419.
(41) Hedberg, L.; Ijima, T.; Hedberg, K. *J. Chem. Phys.* **1979**, *70*, 3224.
(42) (a) Housecroft, C. E.; Wade, K.; Smith, B. C. *J. Chem. Soc., Chem. Commun.* **1978**, 765. (b) Housecroft, C. E.; O'Neill, M. E.; Wade, K.; Smith, B. C. *J. Organomet. Chem.* **1981**, *213*, 35. (c) Conner, J. A. In "Transition Metal Clusters"; Johnson, B. F. G., Ed.; Wiley: New York, 1980.

The heuristic outline of the molecular mechanics calculation (Scheme I) illustrates the use of Δd_{MM} to scale Δd_{MC} by eq 5 and the C–C distances by eq 7 and 8. R_C corresponds to

$$R_C^0 = R_M^0 + (\cos\theta) d_{MC}^0 \quad (7)$$

$$R_C = R_C^0 + (\cos\theta)(\tfrac{1}{2}\Delta d_{MM} + \Delta d_{MC}) \quad (8)$$

the average radius of the spherical surface containing the carbon atoms, R_M is the average radius of the spherical surface containing the metal atoms, and the superscript corresponds to values for $[Fe_4(CO)_{13}]^{2-}$. The angle θ (35.65°) between the threefold axis and one edge of a tetrahedron is used to project the M–C distances onto the radius by eq 7 and the changes in M–M and M–C distances onto the radius in eq 8. The ratio of R_C/R_C' is then the factor by which experimental C–C distances are scaled for any arbitrary value of the M–M distance, the prime superscript corresponding to the radius for $[Fe_3Cr(CO)_{14}]^{2-}$.

Once a value of the strain-free metal–metal distance, d_{MM}^0, is picked, the calculation of energies for a series of M–M distances, d_{MM}, is performed by the procedure outlined in Figure 6. If the parameters are correctly chosen, the resulting total energy (Figure 6, curve 3) should reach a minimum at the observed iron–iron distance. In the present calculations, the d_0 parameter in the C–C nonbonding potential was varied until the total energy minimum correspond to the value of d_{MM} in $[Fe_3Cr(CO)_{14}]^{2-}$ (2.64 Å).

Supplementary Material Available: Complete listings of bond angles and distances (Table XII), positional parameters (Table XIII), anisotropic thermal parameters (Table XIV), and observed and calculated structure factors (40 pages). Ordering information is given on any current masthead page.

Contribution from the Christopher Ingold Laboratories, University College London, London WC1H 0AJ, U.K.

Linear-Chain Halogen-Bridged Mixed-Valence Complexes of Palladium: Infrared, Electronic, Raman, and Resonance Raman Study

ROBIN J. H. CLARK,* VINCENT B. CROUD, and MOHAMEDALLY KURMOO

Received November 4, 1983

The electronic, infrared, and resonance Raman spectra of the linear-chain mixed-valence complexes $[Pd^{II}(LL)_2][Pd^{IV}(LL)_2X_2][ClO_4]_4$, where LL = 1,2-diaminoethane, 1,2-diaminopropane, and 1,3-diaminopropane and X = Cl and Br, are reported. The electronic spectra are characterized in the visible–near-infrared region by intense broad intervalence bands that decrease in wavenumber in the order Cl > Br. The infrared spectra are near-superpositions of those of the constituent ions. The resonance Raman spectra show long overtone progressions ($v_1 v_1$) in the axial $X–Pd^{IV}–X$ symmetric stretching mode (ν_1, which lies at $\simeq$280 cm^{-1} for X = Cl and at $\simeq$150 cm^{-1} for X = Br) and combination tones ($v_1\nu_1 + \nu_n$, where ν_n may be either δ(N–Pd–N) or ν_2, ν_{as} ($X–Pd^{IV}–X$)). The excitation profiles of the ν_1 and $2\nu_1$ bands of the chlorides maximize on the low-energy side of the electronic band maxima, as determined by transmission spectral measurements. For the bromides, enhancement of several bands was observed with red excitation, but none of the excitation profiles reached a maximum even with the excitation line of lowest available wavenumber (799.3 nm ≙ 12 510 cm^{-1}). The palladium complexes were found to have lower intervalence band maxima, ν_1 band excitation profile maxima, and ν_1 values than the analogous platinum complexes. The implications of these results are in agreement with those drawn from conductivity measurements, which indicate that the palladium complexes are the more conducting and thus the ones with the more delocalized valences.

Introduction

Mixed-valence, linear-chain complexes of platinum and palladium are of interest owing to their potential as one-dimensional semiconductors.[1-4] The electronic, infrared, and resonance Raman (RR) spectra of the platinum complexes have been well documented, but little information is yet available on the analogous and potentially more interesting palladium complexes.[5,6] The present investigation is concerned with a spectroscopic study of some cation-chain palladium complexes of the sort

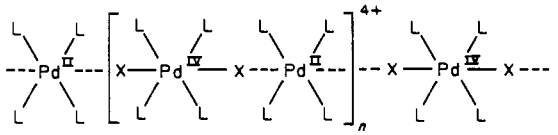

where LL = 1,2-diaminoethane (en), 1,2-diaminopropane (pn), and 1,3-diaminopropane (tn) and X = Cl and Br. The structures of $[Pd(en)_2][Pd(en)_2X_2][ClO_4]_4$, X = Cl and Br, have been found to be similar to those of their platinum analogues.[7,8] They consist of stacks of nearly planar $[Pd(en)_2]$ units bridged by halide ions. Bridging by chlorine is unsymmetrical, producing an alternation of oxidation states, viz. Pd^{II}---Cl–Pd^{IV}–Cl---Pd^{II}---Cl–Pd^{IV}–Cl---, along the chain direction; bromine also bridges in an unsymmetrical fashion, though it tends to sit closer to the midpoint between successive Pd atoms. All the complexes are therefore class II mixed-valence species,[9] and they have been found to be more conducting than their platinum analogues, the bromides being better conductors than the chlorides.[3,10]

Experimental Section

Preparations. Monomers. $[Pd(LL)_2]Cl_2$ was prepared by the method of Bekaroglu et al.[11] $[Pd(en)_2Cl_2][ClO_4]_2$ was obtained by a method different from that originally given by Mason;[12] chlorine gas was bubbled through an aqueous solution of $[Pd(en)_2]Cl_2$ containing an excess of perchloric acid in an ice bath. Addition of cold absolute ethanol led to the slow precipitation of the yellow complex

(1) Brown, D. B., Ed. "Mixed-Valence Compounds"; Reidel: Dordrecht, The Netherlands, 1982.
(2) Clark, R. J. H. *Ann. N.Y. Acad. Sci.* **1978**, *313*, 672.
(3) Aoki, R.; Hamaue, Y.; Kida, S.; Yamashita, M.; Takemura, T.; Furuta, Y.; Kawamori, A. *Mol. Cryst. Liq. Cryst.* **1982**, *81*, 301.
(4) Miller, J. S., Ed. "Extended Linear Chain Compounds"; Plenum Press: New York, 1982, Vols. 1 and 2; *Ibid.* Plenum Press, New York, 1983; Vol. 3.
(5) Clark, R. J. H. *Adv. Infrared Raman Spectrosc.* **1983**, *11*, 95.
(6) Papavassiliou, G. C.; Layek, D.; Theophanides, T. *J. Raman Spectrosc.* **1980**, *9*, 69.
(7) Beauchamp, A. L.; Layek, D.; Theophanides, T. *Acta Crystallogr., Sect. B: Struct. Crystallogr. Cryst. Chem.* **1982**, *B38*, 1158.
(8) Clark, R. J. H.; Croud, V. B.; Kurmoo, M.; Hursthouse, M., unpublished results.
(9) Robin, M. B.; Day, P. *Adv. Inorg. Chem. Radiochem.* **1967**, *10*, 247.
(10) Hamaue, Y.; Aoki, R.; Yamashita, M; Kida, S. *Inorg. Chim. Acta* **1981**, *54*, L13.
(11) Bekaroglu, O.; Breer, H.; Endres, H.; Keller, H. J.; Gung, N. H. *Inorg. Chim. Acta* **1977**, *21*, 183.
(12) Mason, W. R. *Inorg. Chem.* **1973**, *12*, 20.

0020-1669/84/1323-2499$01.50/0